

An Improvement in Synchronously Rotating Reference Frame-Based Voltage Sag Detection under Distorted Grid Voltages

Yutthachai Sillapawicharn* and Yuttana Kumsuwan[†]

Abstract – This study proposed an improvement in synchronously rotating reference frame-based voltage sag detection under distorted grid voltages. In the past, the conventional synchronously rotating reference frame (CSRRF)-based voltage sag detection was generally used in the voltage sag compensation applications. Its disadvantage is a long delay of detection time. The modified synchronously rotating reference frame (MSRRF)-based voltage sag detection is able to detect the voltage sag with only a short delay in detection time. However, its operation under distorted grid voltage conditions is unavailable. This paper proposed the improvement of modified synchronously rotating reference frame (IMSRRF)-based voltage sag detection for use in distorted grid voltages with very fast operation of voltage sag detection. The operation of the proposed voltage sag detections is investigated via simulations and experimentations to verify the performance of the IMSRRF-based voltage sag detection.

Keywords: Voltage sag detection, Synchronously rotating reference frame, Distorted grid voltage

1. Introduction

In recent years, the voltage sag (also called voltage dip in the IEC terminology) has been one of the major factors that affects the quality of the power supply that occurs in a power system. Voltage sag is short duration decrements (between 0.1 pu - 0.9 pu from nominal voltage) in voltage amplitude from one-half to several seconds long. There are reports that 92% of all disturbances in electrical power distribution systems are due to voltage sag, transients, and momentary interruptions [1]. Above 1,500 distinct events from “i-grid.com”, mostly from large industrial plants located around the U.S. and Canada, were studied and analyzed in detail [2]. The study shows that 63% of the disturbances were single-line-to-ground or single-phase faults, 11% were line-to-line or two-phase faults (when single-phase faults and two-phase faults are asymmetrical faults), and 6% were three-phase or symmetrical faults [3]. The voltage sag has a significant influence on non-electronic loads such as induction motors or AC contactors and especially on voltage sensitive loads i.e., electronic loads such as computers, programmable logic controllers (PLC), variable speed drives (VSD), or process control devices, which are all used in modern commercial industry. These disturbances can cause equipment to fail or shut down, which could result in huge losses to the customers.

Several ideas have been reported for compensation or mitigation of voltage disturbances [4-9]. However, in all of

the voltage sag compensation or voltage sag mitigation methods, voltage sag detection is the first essential part of any voltage sag compensation systems since it has to detect voltage sag incidents as fast and initiate the next compensate processes as possible (Fig. 1). If the voltage sag event can be detected in a short time the effects from this voltage sag event can be compensated for, as soon as possible, by the voltage sag compensation system, furthermore, the critical loads will not be affected by this voltage sag. Otherwise the critical loads may be affected if there is a long delay in the detection time in the voltage sag detection process.

There are numerous publications that have proposed voltage sag detection methods and they can be grouped as 1) synchronously rotating reference frame(SRRF)-based, or d-q transformation-based voltage sag detections [10-12], 2) instantaneous voltage technique-based or missing voltage-based voltage sag detections [13, 14], 3) peak voltage evaluation-based voltage sag detections [15, 16], 4)

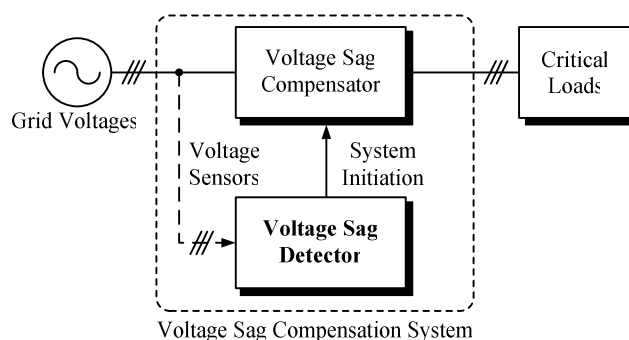


Fig. 1. Typical voltage sag compensation system.

[†] Corresponding Author: Department of Electrical Engineering, Chiang Mai University, Chiang Mai, Thailand. (yt@eng.cmu.ac.th)

* Department of Electrical Engineering, Chiang Mai University, Chiang Mai, Thailand. (ysil72@hotmail.com)

Received: July 27, 2012; Accepted: June 10, 2013

rms evaluation-based voltage sag detections [17, 18], 5) time-frequency transformation-based voltage sag detections [19, 20], 6) rectified voltage-based voltage sag detections [21] and 7) fractal-based voltage sag detections [22, 23].

However, the SRRF-based voltage sag detections are widely used due to their easy implementation. This is because of the SRRF-based voltage sag detections can acquire the existing information about d-q transformation that is available in most voltage sag compensation system control algorithms. The complicated calculation algorithm is unnecessary in the SRRF-based voltage sag detections, whereas it is necessary in other methods.

In the past years, the employment of a popular approach, i.e., conventional synchronously rotating reference frame (CSRRF)-based voltage sag detection, has caused very large delay time from using a low cut-off frequency of low-pass filter (LPF) [24]. This LPF is used to eliminate the 2ω or 100-Hz component (for 50-Hz electrical power distribution systems) from the SRRF-based transformation in unbalance voltage sag conditions.

A shorter delay time can be achieved using modified synchronously rotating reference frame (MSRRF)-based voltage sag detection [12] that employs the 2ω component rejection. This approach gives a very short detection time when compared to the CSRRF-based voltage sag detection. However, the MSRRF-based voltage sag detection can be used only in the ideal grid voltages. In the case of practice, the grid voltages contain harmonics and then the distorted grid voltages appear. These harmonics influence to the operation of MSRRF-based voltage sag detection and therefore failed detection may occur [25].

This paper proposed an improvement on the MSRRF (IMSRRF)-based voltage sag detection that could be operated under distorted grid voltages, with a short delay of detection time in comparison to conventional methods, and it can be used in voltage sag compensation applications.

2. Synchronously Rotating Reference Frame-Based Voltage Sag Detections

2.1 Conventional synchronously rotating reference Frame-based voltage sag detection

The CSRRF-based voltage detection is shown in Fig. 2. This voltage sag detection method utilizes the d-q transformation that gives DC quantities (V_d, V_q) proportion to AC quantities of the grid voltages (V_a, V_b, V_c) or ($V_{s,abc}$) which can be expressed as

$$\begin{pmatrix} V_d \\ V_q \end{pmatrix} = \frac{2}{3} \begin{pmatrix} \cos \omega t & -\sin \omega t \\ \sin \omega t & \cos \omega t \end{pmatrix} \begin{pmatrix} 1 & -1/2 & -1/2 \\ 0 & \sqrt{3}/2 & -\sqrt{3}/2 \end{pmatrix} \begin{pmatrix} V_a \\ V_b \\ V_c \end{pmatrix}. \quad (1)$$

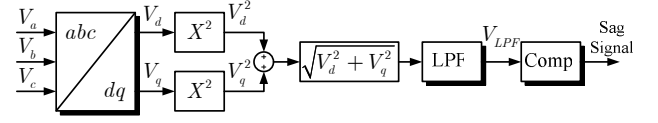
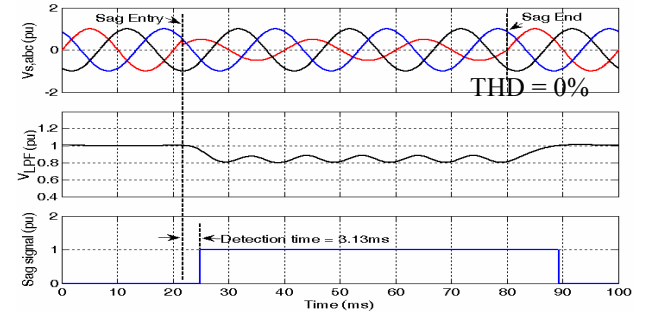
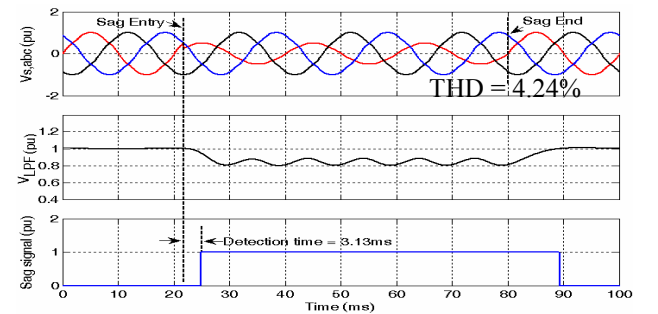


Fig. 2. CSRRF-based voltage sag detection.

From Fig. 2, $V_{dq} = \sqrt{V_d^2 + V_q^2}$, this voltage varies with the grid voltages, then the voltage sags can be detected from the value of V_{dq} . This V_{dq} is filtered by LPF for 2ω or 100-Hz component elimination (for 50-Hz electrical power distribution systems). The filtered V_{dq} or V_{LPF} is finally compared to a DC reference in the comparator. The comparator output is a sag signal, which initiates a voltage sag compensation process when voltage sag occurs. The corresponding simulation waveforms of CSRRF-based voltage sag detection under ideal grid voltages, are shown in Fig. 3(a). This simulation was made with 0.5-pu single-phase voltage sag, 30 degrees of point-on-wave (POW) initiation of voltage sag, and a LPF cut-off frequency at 50 Hz. The voltage sag detection time in this case was 3.13 ms. It can be seen that the large delay of voltage sag detection time was introduced by the low cut-off frequency of LPF. Fig. 3(b) presents the waveforms that are simulated under distorted grid voltages (4.24% THD), in the same condition as in Fig. 3(a). Even the CSRRF-based voltage sag detection is still working in distorted grid voltage, yet the delay of detection time is still long.



(a)



(b)

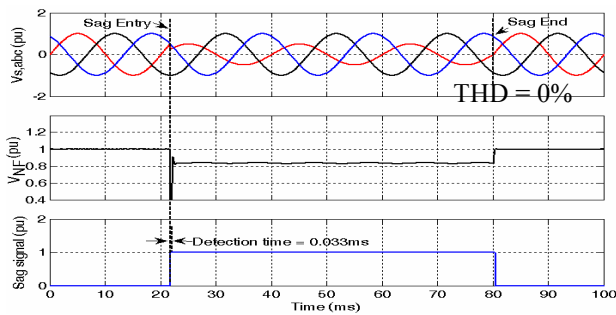
Fig. 3. Simulation results of CSRRF-based voltage sag detection at 0.5-pu single-phase voltage sag and 30 degrees POW initiation: (a) Under ideal grid voltages; (b) Under distorted grid voltages.

2.2 Modified synchronously rotating reference Frame-based voltage sag detection

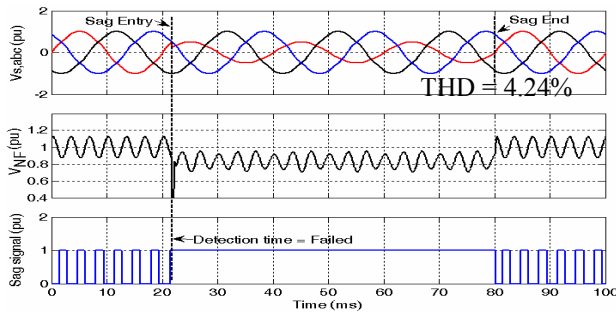
In [12] the MSRRF-based voltage detection was proposed. This voltage sag detection method also utilizes the d-q transformation, in which the differentiator is an additional part. The operation of MSRRF-based voltage sag detection is based on 2ω component cancellation. In this method, the phase of q-axis voltage is shifted by -90 degrees by a differentiator and then added to d-axis voltage.

The 2ω component is then eliminated and this result is filtered by the noise filter (NF) to remove the high frequency components that are due to the discrete differentiator. The NF output voltage V_{NF} is finally compared to a DC reference in the comparator to generate the sag signal. The main function of LPF in MSRRF-based voltage sag detection is filtering the components of differential results due to using of a discrete differentiator where a high cut-off frequency can be selected.

To present the operation of MSRRF-based voltage sag detection, the simulation is made in the condition of 0.5-pu single-phase voltage sag, 30 degrees of POW initiation, and the 2 kHz of NF cut-off frequency. The simulation waveforms of MSRRF-based voltage sag detection under ideal grid voltage are shown in Fig. 4(a). The voltage sag detection time in this case was $33 \mu s$ or 0.033 ms. A very short delay in voltage sag detection time was achieved. In the case of operation under a distorted grid voltage, Fig.



(a)



(b)

Fig. 4. Simulation results of MSRRF-based voltage sag detection at 0.5-pu single-phase voltage sag and 30 degrees POW initiation: (a) Under ideal grid voltages; (b) Under distorted grid voltages.

4(b) shows that the sag signal is an improper signal. This failure of the voltage sag detection process is due to the effect of high frequency components of grid harmonic voltages on the differentiator frequency responses. The differentiator amplifies the high frequency components and generates the faulty sag signal. This is such a serious issue as it cannot be used in distorted grid voltages.

3. Proposed Improved Modified Synchronously Rotating Reference Frame-Based Voltage Sag Detection

Fig. 5 shows the proposed IMSRRF-based voltage sag detection. In spite of the fact that the MSRRF-based voltage sag detection provides a very short delay in detection time, it cannot be operated under distorted grid voltages. In that case, the differentiator is influenced by harmonic components due to the fact that the action of the differentiator is more sensitive with high frequency components.

In Fig. 6, the example waveforms of V_d and V_q in the case of 0.5-pu single-phase voltage sag are illustrated. It can be seen that both of V_d and V_q contain the same amplitude of 2ω components but in different phases. The differential result of V_q (when using phase of V_d as reference) is V'_q which is as follows

$$V'_q = -2\omega V_{qm} \sin(2\omega t) \quad (2)$$

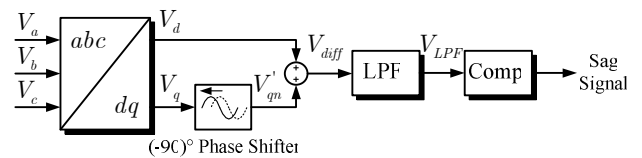


Fig. 5. IMSRRF-based voltage sag detection.

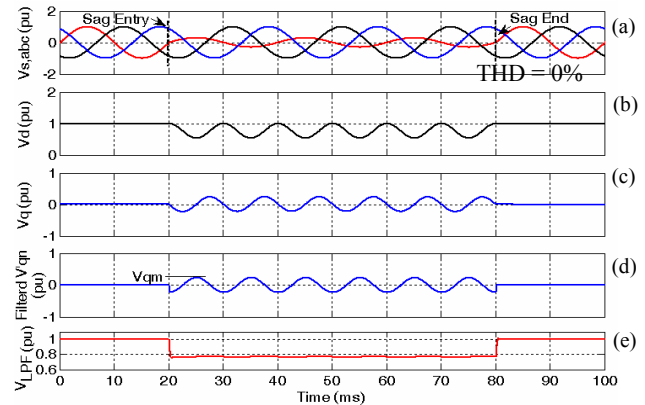


Fig. 6. Example waveforms of IMSRRF operation with 0.5-pu single-phase voltage sag and 0 degrees of POW initiation.

and a constant value of $1/2\omega$ is used to obtain the V'_q normalization value, V'_{qn}

$$V'_{qn} = \frac{V'_q}{2\omega} = -V_{qm} \sin(2\omega t) \quad (3)$$

It can be noticed that the differentiator is actually used for phase shifting of V'_q , then both of V'_{qn} and V'_d have the same amplitude and 180° out-of-phase of 2ω components. Finally, these 2ω components are eliminated V'_d and V'_{qn} , then V_{diff} is obtained as follows

$$V_{diff} = V'_d + V'_{qn} \quad (4)$$

The V_{diff} signal is filtered by LPF with a high cut-off frequency which is defined by V_{LPF} and shows in Fig. 6(e) and it is then compared with a DC reference to generate the sag signal.

In MSRRF-based voltage sag detection, the NF is only used for filtering the high frequency components that comes from differential result. In practical cases, the grid voltages contain harmonics, of which the most existing harmonic components in the practical grid voltages are the fifth harmonic (250 Hz) in a negative sequence and the seventh harmonic (350 Hz) in a positive sequence and they then appear as the sixth order harmonic (300 Hz) [26] in SRRF. Other existing higher frequencies of harmonics are the eleventh harmonic (550 Hz) in a negative sequence and the thirteenth harmonic (650 Hz) in a negative sequence and they then appear as the twelfth order harmonic (600 Hz) Therefore the differential resultant component is increased greatly and the sag signal is invalid.

To figure out this problem then the issue of LPF cut-off frequency (f_c) is designed, taking into account harmonic frequencies. However, in the design criteria will consider only the lowest frequency or 300-Hz component and the higher frequency is not needed to be taken into account, due to the frequency response of LPF.

To filter out this 300-Hz component, the second order LPF is chosen and the LPF cut-off frequency (f_c) is determined at 150 Hz as (5), where f is grid voltage frequency.

$$f_c = \frac{6f}{2} \quad (5)$$

The second order LPF has attenuation gain at -12 dB/octave then the attenuation gain of LPF at frequency of 300 Hz is -12 dB (4-times attenuation).

Other issues concerned with the limits of the hysteresis comparator. As the voltage sag definition, the AC voltages between 0.1 pu - 0.9 pu, from a nominal $\overline{V_{LPF}}$ voltage, are considered to be the voltage sag. Since the $\overline{V_{LPF}}$ voltage (local averaging value of V_{LPF}) varies with three-phase AC voltages as expressed in (6).

$$\overline{V_{LPF}}(pu) = \frac{Va(pu) + Vb(pu) + Vc(pu)}{3} \quad (6)$$

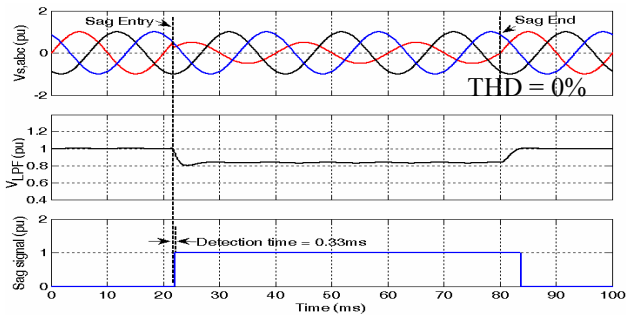
This voltage is compared to certain amounts of comparator limits that create the sag signal. The limits consist of lower and upper limits, when the lower limit of hysteresis comparator is assigned for a normal-to-sag state transition and the upper limit is assigned for sag-to-normal state transition. The lower and upper limits of the hysteresis comparator are mostly set at 0.9 pu and 1.0 pu, respectively. The detection range of voltage sag can be calculated from (6). In the case of lower limit is set to 0.9 pu then the lowest amount of single-phase voltage sag (caused by single-phase-to-ground fault) that can be detected is 0.7 pu, the lowest amount of two-phase voltage sag (caused by line-to-line fault) that can be detected is 0.85pu, and the lowest amount of three-phase voltage sag (caused by symmetrical fault) that can be detected is 0.9 pu. It can be noticed that the single-phase voltage sag cannot be detected in the range between 0.7 pu- 0.9 pu and the two-phase voltage sag cannot be detected in the range between 0.85 pu - 0.9 pu.

The single-phase voltage sag is actually the most frequent event, however, and it should be emphasized more than other cases. Then the lower limit of hysteresis comparator is aimed to be to set as high as possible to get the 0.9 pu of $\overline{V_{LPF}}$.

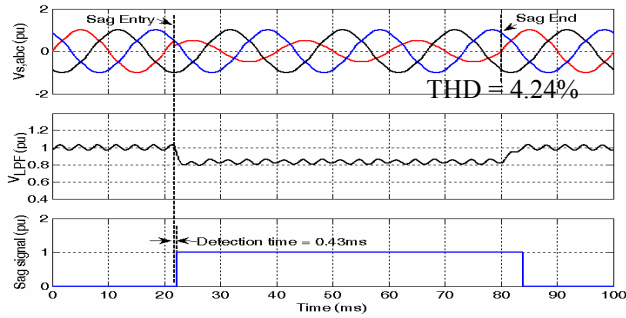
However, there is another factor that should be taken into account. The high value of comparator's lower limit makes it more sensitivity of two-phase and three-phase voltage sag detection i.e., the two-phase and three-phase voltage sag that are higher than 0.9 pu are considered as sag.

To meet the requirement of a single-phase voltage sag detection, the lower limit of the hysteresis comparator was chosen at 0.95 pu and then the lowest detected value of voltage sag in each type is 0.85 pu, 0.925 pu, and 0.95 pu for the single-phase voltage sag, two-phase voltage sag, and three-phase voltage sag, respectively. It can be seen that in the case of single-phase voltage sag, the lowest detected value of voltage sag is higher than the value of sag definition by 0.05 pu; in the case of three-phase voltage sag, the lowest detected value is lower than the value of sag definition by 0.05 pu. Finally, the upper limit is set to 1.0 pu to avoid oscillations of the sag signal.

The simulation waveforms of IMSRRF-based voltage sag detection under ideal grid voltage are depicted in Fig. 7(a). To demonstrate the operation of MSRRF-based voltage sag detection, the condition of 0.5-pu single-phase voltage sag, 30 degrees of POW initiation, and the cut-off frequency of LPF is 150 Hz, as was determined in the simulation. The voltage sag detection time in this case was 0.33 ms. The detection time of IMSRRF-based voltage sag detection is ten times that of the detection time of MSRRF-based voltage sag detection in the case of an ideal grid voltage. In the case of operations under distorted grid



(a)



(b)

Fig. 7. Simulation results of IMSRRF-based voltage sag detection at 0.5-pu single-phase voltage sag and 30 degrees POW initiation: (a) Under ideal grid voltages; (b) Under distorted grid voltages.

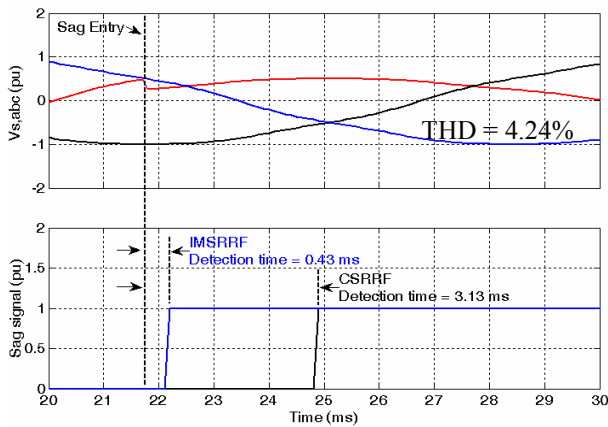


Fig. 8. Voltage sag detection time comparison for single-phase voltage sag under distorted grid voltage between CSRRF-based and IMSRRF-based voltage sag detection.

voltage, however, it can be shown from Fig. 7(b) that the operation of IMSRRF-based voltage sag detection was still properly working and gave a short delay in detection i.e., 0.43 ms when compared to the CSRRF-based voltage sag detection.

In Fig. 8, it shows the comparison of voltage sag detection times of CSRRF-based and IMSRRF-based voltage sag detection under distorted grid voltage in the

Table 1. Parameters of voltage detection system

Grid phase voltages (V_a, V_b, V_c)	220 Vrms, 50 Hz
Grid voltages distortion, THD	4.24% THD. (hd5 = 3%, hd7 = 3%)
Voltage sags	Single-phase, 0.5 pu, 0.7 pu Three-phase, 0.5 pu, 0.7 pu Unbalance phase, 0.5 pu
Point-on-wave initiation of voltage sags	41 degrees, 131 degrees
Cut-off frequency of low pass filters, f_c	150 Hz
Comparator hysteresis band	Lower limit = 0.95 Upper limit = 1.0
Controller	dSpace DS1104
Controller data sampling time	100 μ s
Voltage sag generator	California Instruments 4500LS

condition of 0.5-pu single-phase voltage sag, and 30 degrees of POW initiation.

4. Results and Discussions

The model of the voltage sag detection of Fig. 5 was built by using Matlab/Simulink simulation software. The simulation model was developed based on voltage sag detections under distorted grid voltages in single-phase voltage sag conditions, two-phase voltage sag conditions with phase-angle jump, and three-phase voltage sag conditions. The total harmonic distortion (THD) of the grid voltage under the proposed model is set to 4.24%, which consists of 3% of the fifth harmonic in a negative sequence and 3% of the seventh harmonic in a positive sequence. These conditions are based on harmonic limit standards of IEEE 519-1992 and the IEC standard 61000-3-6. The experimental setup is shown in Fig. 9. The system parameters for simulation and experimentation of the voltage sag detections are given in Table 1.

4.1. Asymmetrical voltage sag cases

The operation waveforms of IMSRRF-based voltage sag detection under asymmetrical voltage sag i.e., single-phase voltage sag and 4.24% THD of grid voltage, are illustrated in Figs. 10 to 13 with various conditions of sag depth and degrees of POW initiation to prove the performance of the proposed IMSRRF-based voltage sag detection.

Fig. 10(a) shows the simulation results of the grid phase voltages ($V_{s,abc}$), filtered LPF output voltage 0.5-pu single-phase voltage sag, and 41 degrees of POW initiation. It can be seen from V_{LPF} that, while the 100-Hz component disappears due to 2ω component cancellation, the high frequency component due to grid harmonic voltage still exists. However, with a suitable cut-off frequency for LPF, the high frequency component from the harmonic voltage and the differentiator action is mitigated. The proper sag signal is finally obtained, as seen in Fig. 10(a), with a short

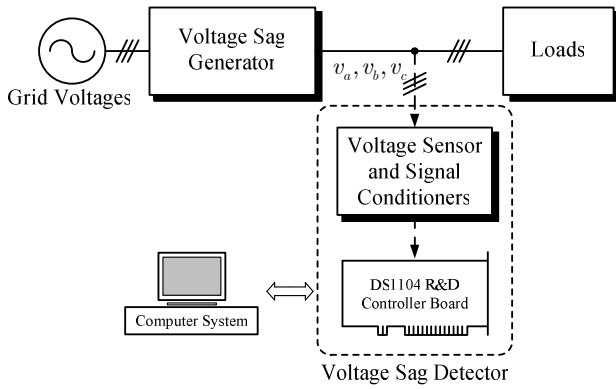


Fig. 9. Experimental setup.

delay of detection time i.e., 0.222 ms.

To verify the simulation results in Fig. 10(a), the experimentation with the same conditions was conducted and illustrated in Fig. 10(b). The detection time from the experimental results was 0.28 ms, which is close to the simulation results.

Fig. 11(a) depicts the simulation results of the grid phase voltage (V_{LPF}), and sag signal for operation with 0.5-pu single-phase voltage sag and 131 degrees of POW initiation. The delay of detection time is 2.12 ms. It can be noticed that in condition of single-phase voltage sag, the delay of detection time moderately depends on POW initiation. These simulation results are proved by the experimental results, which are shown in Fig. 11(b). The voltage sag detection in this case is also 2.12 ms

Fig. 12(a) presents the simulation results for operation with 0.7-pu single-phase voltage sag and 41 degrees of POW initiation. The delay in detection time in this simulation condition was 0.322 ms. It can be seen that there is still a brief delay in detection time. These simulated results indicate that the delay in detection time rarely depends on sag depth. The detection time from the experimental results was 0.36 ms as shown in Fig. 12(b).

Fig. 13(a) illustrates the simulated results for operation with 0.7-pu single-phase voltage sag and 131 degrees of POW initiation. In this case, the delay in detection time was 2.32 ms. These simulation results are verified by the experimental results in Fig. 13(b) and detection time was 2.12 ms.

For more explanation about the operation of IMSRRF-based voltage sag detection, more simulation and experimental conditions are made. The simulation and experimental conditions are numerous values of sag depth (0.3 pu, 0.5 pu, and 0.7 pu), numerous types of asymmetrical voltage sag (single phase and two phase), and numerous degrees of POW initiation (0 - 360 degrees in step of 9 degrees).

The simulation and experimental results are shown in Fig. 14. Fig. 14(a) it illustrates the simulation and experimental result of the most probable event i.e., the single-phase voltage sag. It can be seen that the delay of

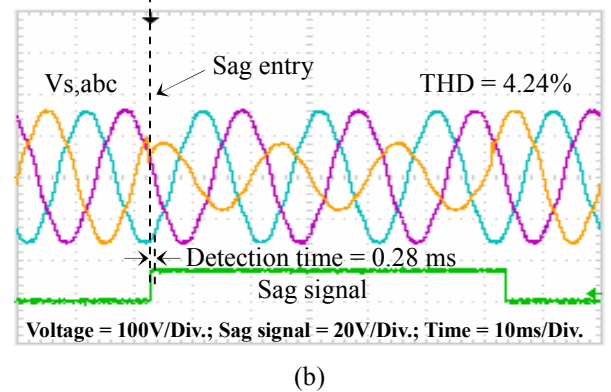
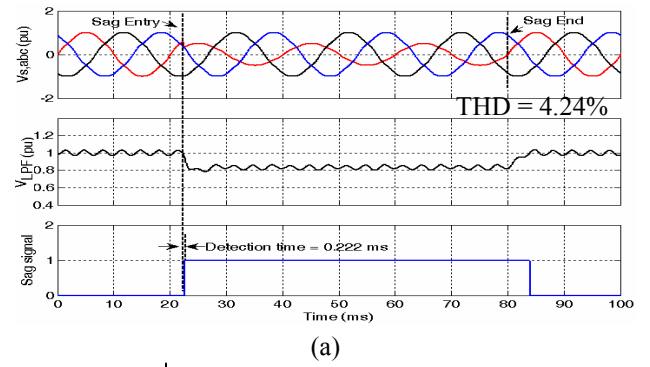


Fig. 10. Operation results under distorted grid voltages of IMSRRF-based voltage sag detection with 0.5-pu single-phase voltage sag and 41 degrees of POW initiation: (a) Simulation; (b) Experimentation.

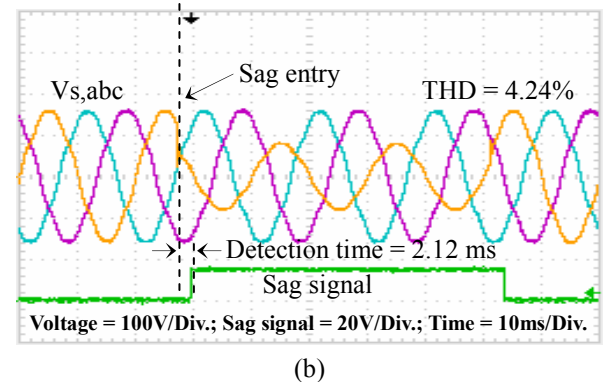
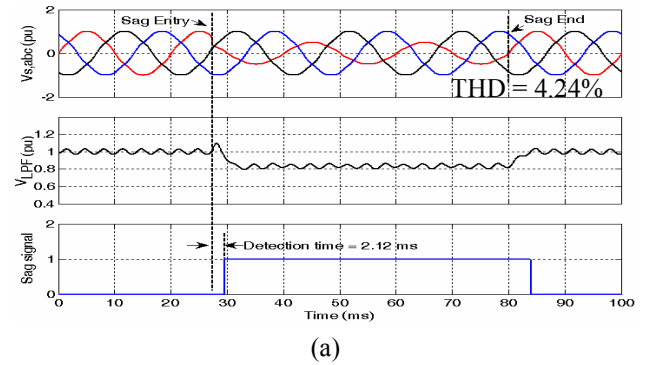


Fig. 11. Operation results under distorted grid voltages of IMSRRF-based voltage sag detection with 0.5-pu single-phase voltage sag and 131 degrees of POW initiation: (a) Simulation; (b) Experimentation.

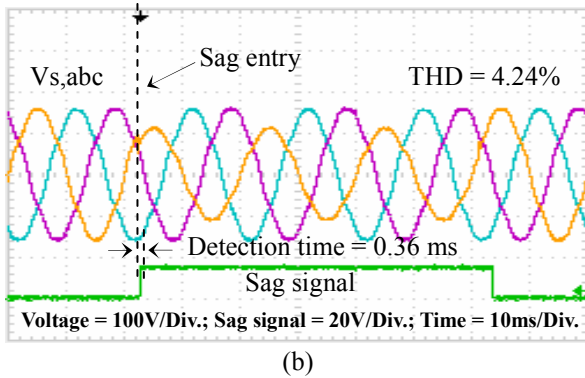
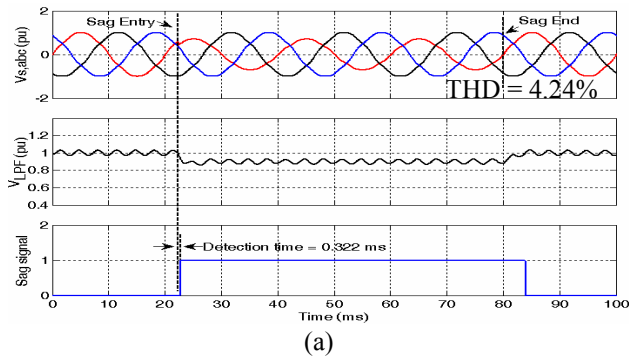


Fig. 12. Operation results under distorted grid voltages of IMSRRF-based voltage sag detection with 0.7-pu single-phase voltage sag and 41 degrees of POW initiation: (a) Simulation; (b) Experimentation.

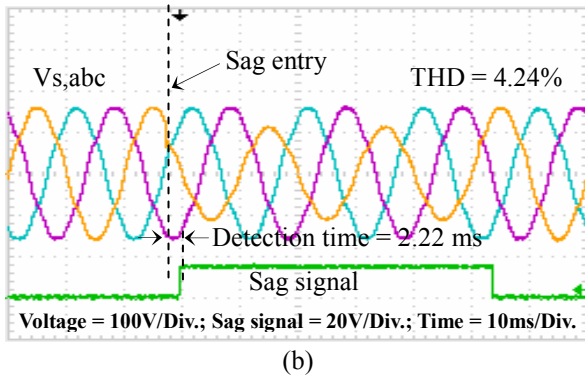
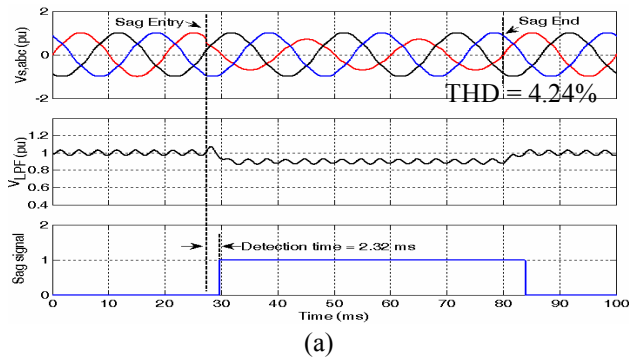


Fig. 13. Operation results under distorted grid voltages of IMSRRF-based voltage sag detection with 0.7-pu single-phase voltage sag and 131 degrees of POW initiation: (a) Simulation; (b) Experimentation.

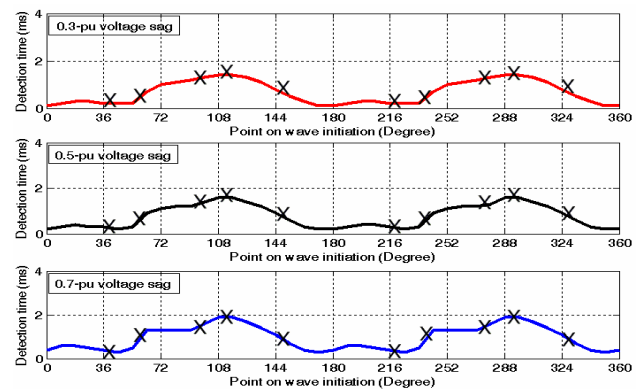
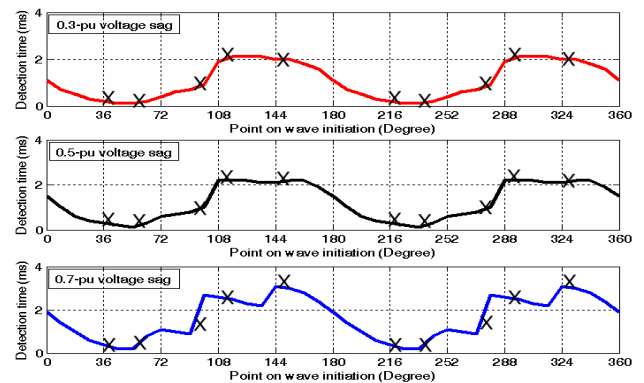


Fig. 14. Simulation and experimental results for operation under distorted grid voltages of IMSRRF-based voltage sag detection with asymmetrical voltage sag in function of POW initiation: (a) Single-phase voltage sag; (b) Two-phase voltage sag.

detection time varies with degrees of POW initiation.

The operation results of IMSRRF-based voltage sag detection under the two-phase voltage sag are shown in Fig. 14(b).

It can be seen that the maximum detection time noticeably reduce when compared to single-phase voltage sag. It can be noticed that in the case of single-phase voltage sag, the detection times are more affected by POW initiations than sag depths. The shortest or best detection times and longest or worst detection times are summarized in Table 2.

Table 2. Summary of asymmetrical voltage detection times from simulation results.

Sag types	Best detection times (ms)			Worst detection times (ms)		
	Sag depth (pu)			Sag depth (pu)		
	0.3	0.5	0.7	0.3	0.5	0.7
1-phase Asymmetry	0.1	0.1	0.2	2.1	2.3	3.2
2-phase Asymmetry	0.1	0.2	0.2	1.4	1.6	2.0

4.2. Symmetrical voltage sag cases

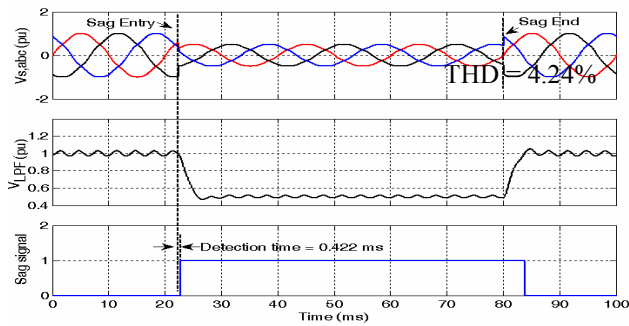
The simulation waveforms in Figs. 15 to 18 are used for an explanation of IMSRRF-based voltage sag detection operation under symmetrical voltage sag i.e., three-phase voltage sag and 4.24% THD of grid voltage. These simulations are assigned to various conditions of sag depth and degrees of POW initiation to certify the functioning of the proposed IMSRRF-based voltage sag detection.

The simulation waveforms in condition of 0.5-pu three-phase voltage sag and 41 degrees of POW initiation are indicated in Fig. 15(a). It can be noticed that in the case of three-phase voltage sag, the V_{LPF} decreases more than in the case of single-phase voltage sag as described in (6). The exact operation in this case also takes place as seen in the sag signal in Fig. 15(a) with a 0.422 ms detection time. This is an almost identical value to the detection time from the experimental results shown in Fig. 15(b), which is 0.4 ms. By only changing the POW initiation to 131 degrees, the other conditions of the simulation are still preserved then the delay in detection time is 0.622 ms, as seen in the result waveforms in Fig 16(a). It can be clearly seen that the delay in detection time rarely depends on the varying degrees of POW initiation in terms of three-phase voltage sag. These simulation results were checked by experimental results as illustrate in Fig. 16(b). The experimental

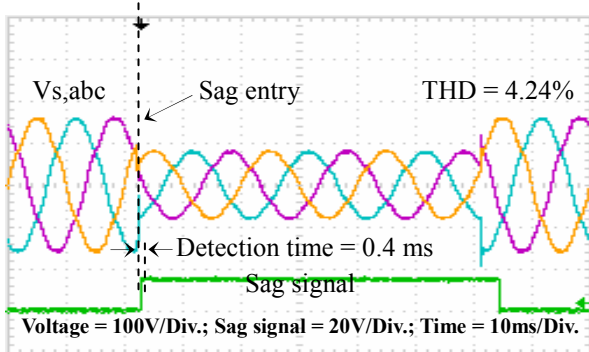
detection time was 0.8 ms.

To find out a relation between the delay of detection time and sag depth in three-phase voltage sag, the simulation was established with 0.7-pu three-phase voltage sag and 41 degrees of POW initiation, and the resulting waveforms are shown in Fig. 17(a). The sag signal has a delay in detection time equal to 0.522 ms, this can be seen in that the delay of detection time seldom depends on sag depth, in the case of three-phase. The experimental results under the same conditions are presented in Fig. 17(b). It can be seen that the experimental detection time was 0.54 ms.

In Fig. 18(a), the simulation condition was set with 0.7 pu sag depth and 131 degrees of POW initiation. The delay in detection time was 0.922 ms and the experimental detection time is 1.06 ms, as seen in Fig. 18(b). These simulation and experimental results confirmed that a delay in detection time rarely depends on sag depth in the three-phase case. For more explanation about the operation of IMSRRF-based voltage sag detection, more simulation and experimental conditions were made. The simulation and experimental conditions were numerous values of sag depth (0.3 pu, 0.5 pu, and 0.7 pu), and numerous degrees of POW initiation (0 - 360 degrees in step of 9 degrees). The simulation and experimental results are shown in Fig. 19.

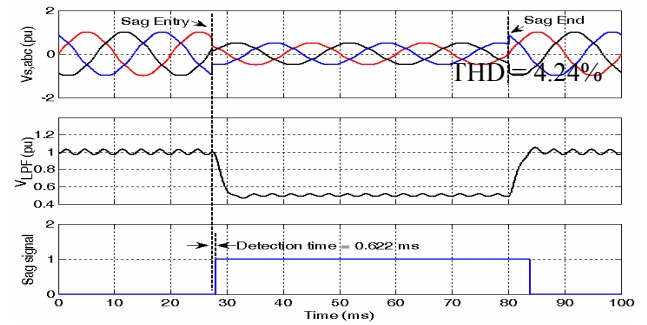


(a)

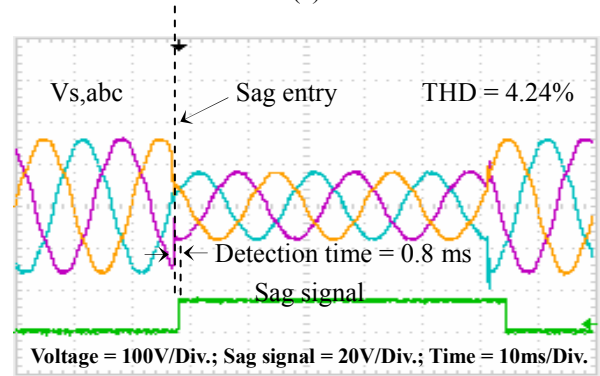


(b)

Fig. 15. Operation results under distorted grid voltages of IMSRRF-based voltage sag detection with 0.5-pu three-phase voltage sag and 41 degrees of POW initiation: (a) Simulation; (b) Experimentation.

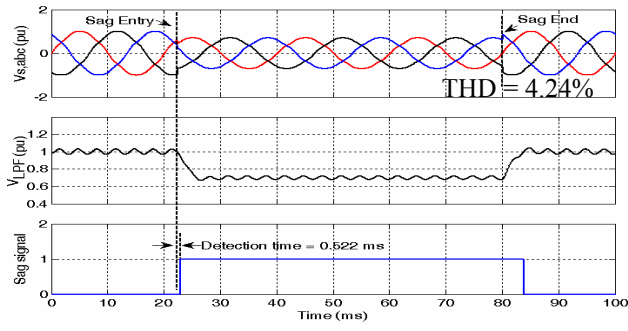


(a)

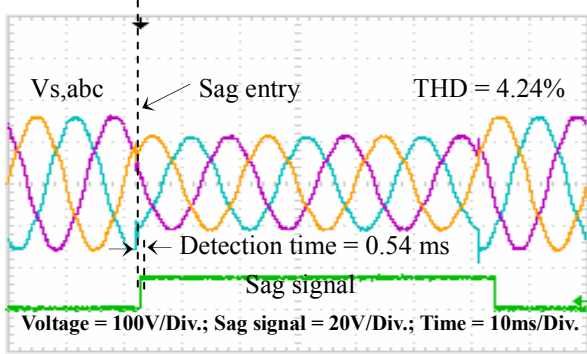


(b)

Fig. 16. Operation results under distorted grid voltages of IMSRRF-based voltage sag detection with 0.5-pu three-phase voltage sag and 131 degrees of POW initiation: (a) Simulation; (b) Experimentation.

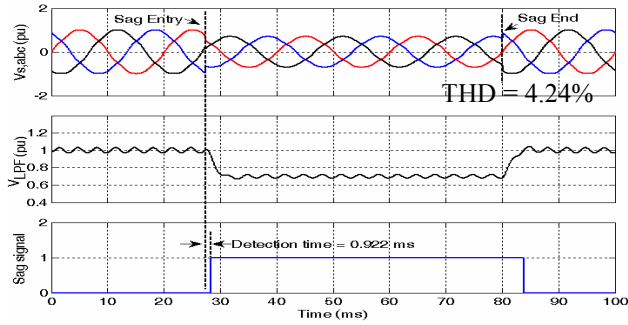


(a)

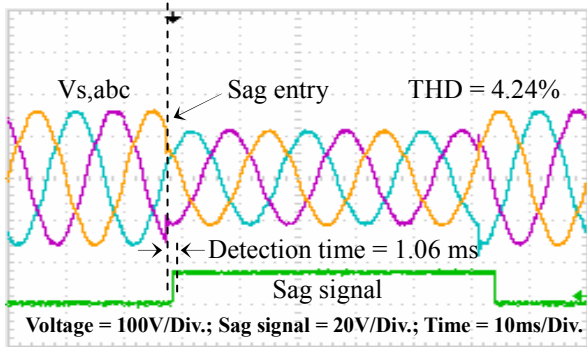


(b)

Fig. 17. Operation results under distorted grid voltages of IMSRRF-based voltage sag detection with 0.7-pu three-phase voltage sag and 41 degrees of POW initiation. (a) Simulation. (b) Experimentation.



(a)



(b)

Fig. 18. Operation results under distorted grid voltages of IMSRRF-based voltage sag detection with 0.7-pu three-phase voltage sag and 131 degrees of POW initiation. (a) Simulation. (b) Experimentation.

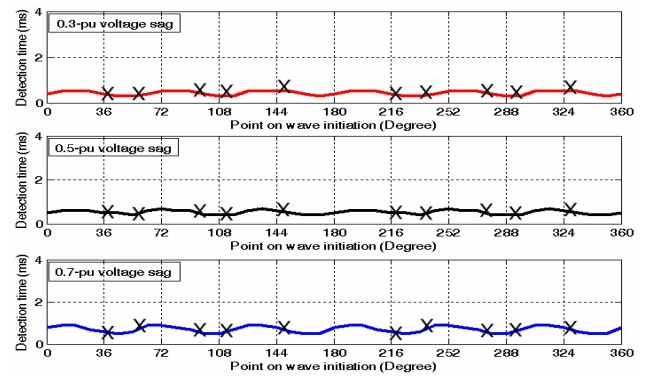


Fig. 19. Simulation and experimental results for operation under distorted grid voltages of IMSRRF-based voltage sag detection with symmetrical or three-phase voltage sag in function of POW initiation.

Table 3. Summary of symmetrical voltage sag detection times from simulation results.

Sag type	Best detection times (ms)			Worst detection times (ms)		
	Sag depth (pu)			Sag depth (pu)		
	0.3	0.5	0.7	0.3	0.5	0.7
3-phase Symmetry	0.3	0.3	0.4	0.5	0.7	0.9

In Fig. 19 presents the operation results of IMSRRF-based voltage sag detection under the three-phase voltage sag. It can be seen that the greatest delay in detection time obviously decreases when comparing it to single-phase voltage sag and two-phase voltage sag. It can be seen that the detection times, in the case of three-phase voltage sag, fluctuates less than in the case of single-phase and two-phase voltage sags. Table 3 summarizes the shortest or best detection times, and longest or worst detection times in symmetrical voltage sag.

4.3. Effect of unbalance phase voltage sag

The operational waveforms of IMSRRF-based voltage sag detections under unbalance phase voltage sag with 0.5 pu sag depth and various degrees of POW initiation are depicted in Figs. 20 and 21 to show the performance of the proposed voltage sag detection. In these cases, the grid voltages are seen as a reduction of the voltage in two phases. The phase of voltage is lagging by 15 degrees in phase B (i.e. 225 degrees), and leading by 15 degrees in phase C (i.e. 135 degrees). In Fig. 20, it can be seen that IMSRRF-based voltage sag detection is able to work in unbalance phase voltage sag. With 0.5-pu unbalance phase voltage sag and 41 degrees of POW initiation, the voltage-sag event can be detected in 1.6 ms and 1.62 ms for simulation and experimentation respectively.

In Fig. 21, POW initiation was varied to 141 degrees. In this case the voltage sag can be discovered in 0.3 ms and 0.36 ms for simulation and experimentation respectively.

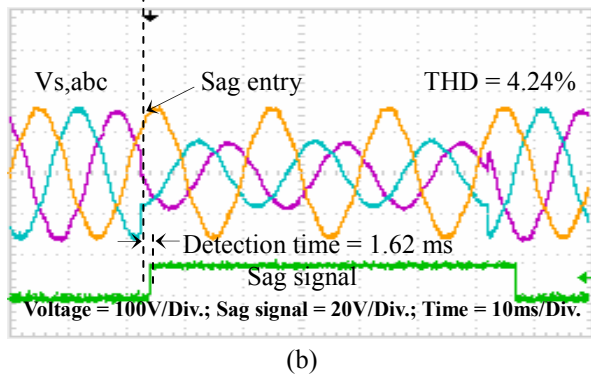
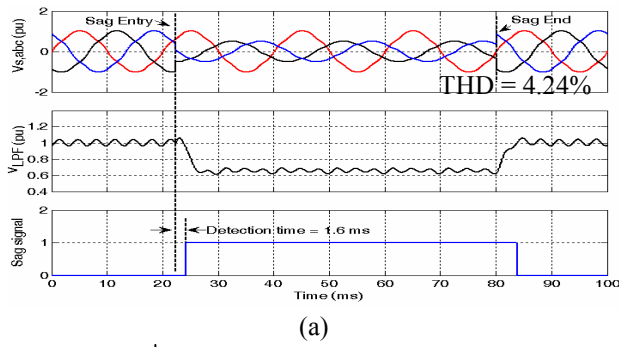


Fig. 20. Operation results under distorted grid voltages of IMSRRF-based voltage sag detection with 0.5-pu unbalance phase voltage sag and 41 degrees of POW initiation: (a) Simulation; (b) Experimentation.

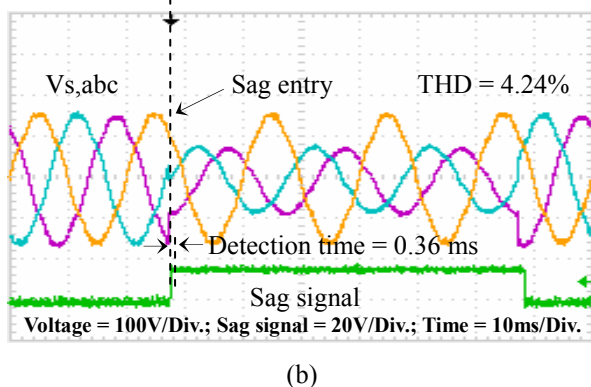
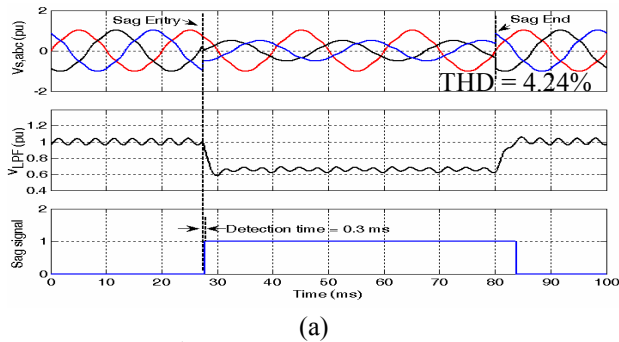


Fig. 21. Operation results under distorted grid voltages of IMSRRF-based voltage sag detection with 0.5-pu unbalance phase voltage sag with and 131 degrees of POW initiation. (a) Simulation. (b) Experimentation.

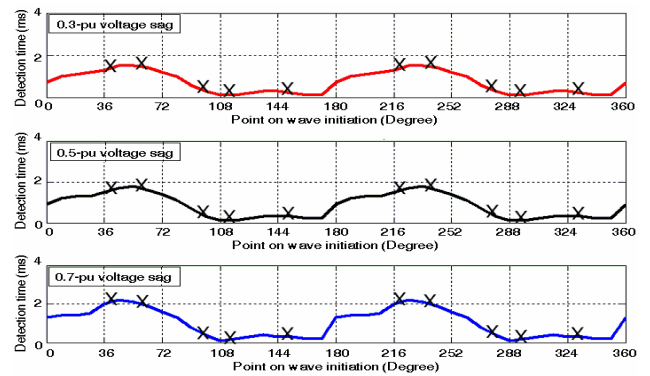


Fig. 22. Simulation and experimental results for operation under distorted grid voltages of IMSRRF-based voltage sag detection with unbalance phase voltage sag in function of POW initiation.

Table 4. Summary of asymmetrical voltage sag with phase-angle jump detection times from simulation results.

Sag type	Best detection times (ms)			Worst detection times (ms)		
	Sag depth (pu)			Sag depth (pu)		
	0.3	0.5	0.7	0.3	0.5	0.7
Unbalance phase	0.1	0.1	0.1	1.5	1.8	2.2

The operation results of IMSRRF-based voltage sag detection under unbalance phase voltage sag are shown in Fig. 22. Table 4 summarizes best detection times, and worst detection times in unbalance phase voltage sag.

4.4 A comparison between proposed IMSRRF-based and CSRRF-based voltage sag detections

A comparison between the proposed IMSRRF-based and CSRRF-based voltage sag detection were made in this section to verify the merit of the proposed voltage sag detection.

In Figs. 23, 24 and 25 show the experimentations of CSRRF-based voltage sag detection under distorted grid voltages with 0.5-pu single-phase, three-phase and unbalance phase voltage sags respectively. It can be easily seen that very large detection times occurred when using the CSRRF-based voltage sag detection. For example, the detection time was 2.8 ms with single-phase voltage sag in Fig. 23 when comparing to 0.28 ms of IMSRRF-based voltage sag detection in Fig. 10(b). With three-phase voltage sag in Fig. 24, the detection time was 1.75 ms when comparing to 0.4 ms of IMSRRF-based voltage sag detection in Fig. 15(b). Finally the detection time was 2.82 ms with unbalance phase voltage sag in Fig. 25 when comparing to 1.62 ms of IMSRRF-based voltage sag detection in Fig. 20(b).

Fig. 26 shows the comparison of IMSRRF-based and CSRRF-based voltage sag detections under various types

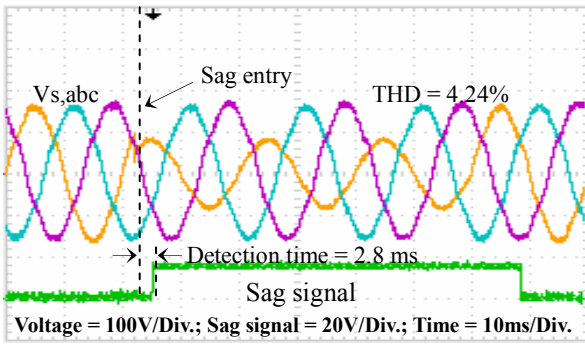


Fig. 23. Experimental results under distorted grid voltages of CSRRF-based voltage sag detection with 0.5-pu single-phase voltage sag and 41 degrees of POW initiation.

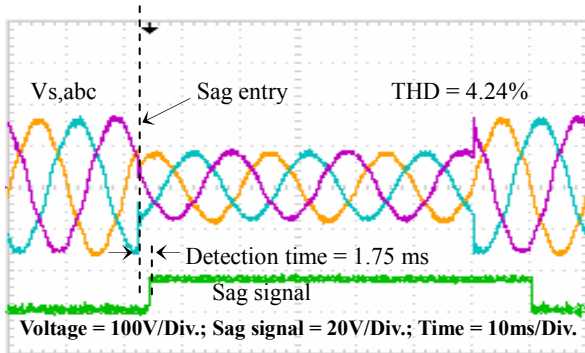


Fig. 24. Experimental results under distorted grid voltages of CSRRF-based voltage sag detection with 0.5-pu three-phase voltage sag and 41 degrees of POW initiation.

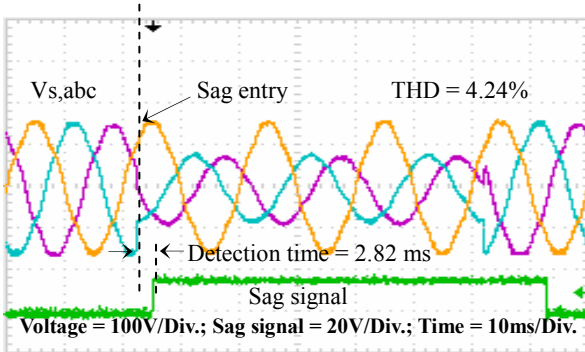


Fig.25. Experimental results under distorted grid voltages of CSRRF-based voltage sag detection with 0.5-pu unbalance phase voltage sag and 41 degrees of POW initiation.

of voltage sag by using simulation results. It can be seen that the good performance in voltage sag detection was presented by the proposed IMSRRF-based voltage sag detection. The proposed voltage sag detection gives the shortest detection time for every type and every POW initiation of voltage sag when comparing to CSRRF-based voltage sag detection.

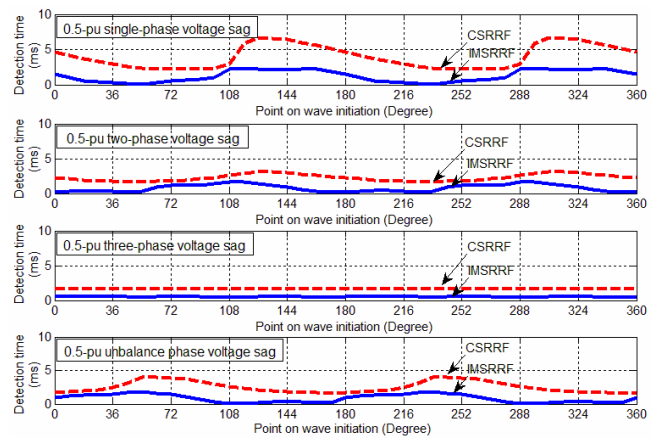


Fig.26. Comparison of simulation results under distorted grid voltages of IMSRRF-based and CSRRF-based voltage sag detections.

5. Conclusion

An improvement in SRRF-based voltage sag detection under distorted grid voltages was proposed in this paper. While CSRRF-based voltage sag detection is already widely used in voltage sag compensation, the long delay of detection time is introduced. This means the next process, initiation of voltage sag compensation, is also delayed, resulting in the voltage sag influencing the load voltage. The MSRRF-based voltage sag detection is able to work with short delay in detection time by use of a differentiator, which works as a 2ω component cancellation. However, it cannot be used in distorted grid voltages due to the frequency response of the differentiator with high frequency voltage components. The investigation into proposed IMSRRF-based voltage sag detection has taken place by reconsideration of its operation under distorted grid voltages. The operation of this proposed IMSRRF-based voltage sag detection was verified by simulation and experimentation in condition of 4.24% THD grid voltage, numerous values of sag depths, numerous values of degrees of POW initiation, and various types of voltage sags. As seen in the simulation and experimental results, this proposed IMSRRF-based voltage sag detection can detect the voltage sag under distorted grid voltage with a very short delay time when compared to the CSRRF and MSRRF-based voltage sag detections. The proposed voltage sag detection can be used in any voltage sag compensation systems to improve their performance.

Acknowledgements

The authors would like to thank financial supports from National Research University (NRU) Project from Office of the Higher Education Commission of Thailand and Energy Conservation Promotion Fund.

References

- [1] D. L. Brooks and D.D. Sabin, "An Assessment of Distribution System Power Quality," Elect. Power Res. Inst., Palo Alto, CA, EPRI Final Rep. TR-106249-V2, May 1996.
- [2] D. Divan, G. A. Luckjiff, W. E. Brumsickle, J. Freeborg and A. Bhadkamkar "A Grid Information Resource for Nationwide Real-time Power Monitoring," *IEEE Trans. Ind. Appl.*, Vol. 40, No. 2, pp. 699-705, Mar. -Apr. 2004.
- [3] A. Prasai and D. M. Divan, "Zero-energy Sag Correctors-optimizing Dynamic Voltage Restorers for Industrial Applications," *IEEE Trans. Ind. Appl.*, Vol. 44, No. 6, pp. 1777-1784, Nov.-Dec. 2008.
- [4] J.G. Nielsen and F. Blaabjerg, "A Detailed Comparison of System Topologies for Dynamic Voltage Restorers," *IEEE Trans. on Ind. Appl.*, Vol. 41, No. 5, pp. 1272-1280, Sept.-Oct. 2005.
- [5] V. Khadkikar, "Enhancing Electric Power Quality Using UPQC: A Comprehensive Overview," *IEEE Trans. on Power Elec.*, Vol. 27, No. 5, pp. 2284-2297, May 2012.
- [6] Y. Sillapawicharn and Y. Kumsuwan, "Voltage Sag Compensation using Two Three-phase Voltage-fed PWM Converters," in *Proceedings of ECTI-CON 2011*, KhonKaen, Thailand, May 2011.
- [7] D. Lee, T. G. Habetle, R. G. Harley, T. L. Keister and J. R. Rostron "A Voltage Sag Supporter Utilizing a PWM-Switched Autotransformer," *IEEE Trans. Power Elec.*, Vol. 22, No. 2, p. 626-635, Mar. 2007.
- [8] O.C. Montero-Hernandez and P.N. Enjeti, "Ride-Through for Critical Load. Exploring a Low-Cost Approach to Maintaining Continuous Connections between Buildings and/or Industrial Systems," *IEEE Ind. Appl. Mag.*, Vol. 8, No. 6, pp. 45-53, Nov.-Dec. 2002.
- [9] S.Subramanian and M.K Mishra, "Interphase AC-AC Topology for Voltage Sag Supporter," *IEEE Trans. on Power Elec.*, Vol. 25, No. 2, pp. 514-518, Feb. 2010.
- [10] Y.H. Chen, C.Y. Lin, J.M. Chen and P.T. Cheng, "An Inrush Mitigation Technique of Load Transformers for the Series Voltage Sag Compensator," *IEEE Trans. on Power Elec.*, Vol. 25, No. 8, pp. 2211-2221, Aug. 2010.
- [11] O.C. Montero-Hernandez and P.N. Enjeti, "A Fast Detection Algorithm Suitable for Mitigation of Numerous Power Quality Disturbances," *IEEE Trans. On Ind. Appl.*, Vol. 41, No. 6, pp. 1684-1690, Nov.-Dec. 2005.
- [12] M. Tumay, M.E. Meral and K.C. Bayindir, "Sequence Reference Frame-based New Sag/swell Detection Method for Static Transfer Switch," *IET Power Elec.*, Vol. 2, No. 4, pp. 431-442, July 2009.
- [13] K.Ding, K.W.E. Cheng, X.D. Xue, B.P. Divakar, C.D. Xu, Y.B. Che, D.H. Wang and P. Dong, "A Novel Detection Method for Voltage Sags," in *Proceedings of ICPESA 2006*, pp. 250-255, Nov. 2006.
- [14] N.S. Tunaboylu, E.R. Collins, Jr. and P.R. Chaney, "Voltage Disturbance Evaluation Using The Missing Voltage Technique," in *Proceedings of Harmonics and Quality of Power*, Oct. 1998.
- [15] H.Y. Chu, H.L. Jou and C.L. Huang, "Transient Response of a Peak Voltage Detector for Sinusoidal Signals," *IEEE Trans. On Ind. Electron.*, Vol. 39, No. 1, pp. 74-79, Feb. 1992.
- [16] S. Lee, T.K. Vu and H. Cha, "A New Fast Peak Detector for Single or Three-phase Unsymmetrical Voltage Sags," in *Proceedings of IEEE-ECCE2010*, Arizona, USA, Sept. 2010.
- [17] D. Gallo, C. Landi and M. Luiso, "Accuracy Analysis of Algorithms Adopted in Voltage Dip Measurements," *IEEE Trans. On Instrum. Meas.*, Vol. 59, No. 10, pp. 2652-2659, Oct. 2010.
- [18] M. Albu and G.T. Heydt, "On the Use of RMS Values in Power Quality Assessment," *IEEE Transactions on Power Del.*, Vol. 18, No. 4, pp. 1586-1587, Oct. 2003.
- [19] R.H.G Tan and V.K. Ramachandaramurthy, "Real Time Power Quality Event Detection using Continuous Wavelet Transform," in *Proceedings of IEEEIC2011*, Rome, Italy, May 2011.
- [20] O. Poisson, P. Rioual and M. Meunier, "Detection and Measurement of Power Quality Disturbances Using Wavelet Transform," *IEEE Trans. On Power Del.*, Vol. 15, No. 3, pp. 1039-1044, Jul. 2000.
- [21] A. Florio, A. Mariscotti and M. Mazzucchelli, "Voltage Sag Detection Based on Rectified Voltage Processing," *IEEE Trans. On Power Del.*, Vol. 19, No. 4, pp. 1962-1967, Oct. 2004.
- [22] S.J. Huang and C.T. Hsieh, "Feasibility of Fractal-based Methods for Visualization of Power System Disturbances," *ELSEVIER International Journal of Electrical Power & Energy Systems*, Vol. 23, No. 1, pp.31-36, Jan. 2001.
- [23] G. Li, M. Zhou, Y. Luo and Y. Ni, "Power Quality Disturbance Detection Based on Mathematical Morphology and Fractal Technique," in *Proceedings of IEEE/PES2005*, Aug. 2005.
- [24] Y.H. Chen, C.Y. Lin, J.M. Chen and P.T. Cheng, "An Inrush Mitigation Technique of Load Transformers for the Series Voltage Sag Compensator," *IEEE Trans. on Power Elec.*, Vol. 25, No. 8, pp. 2211-2221, Aug. 2010.
- [25] Y. Sillapawicharn and Y. Kumsuwan, "An Improvement of Synchronously Rotating Reference Frame-Based Voltage Sag Detection for Voltage Sag Compensation Applications under Distorted Grid Voltages," in *Proceedings of IEEE-PEDS2011*, Singapore, Dec. 2011.
- [26] P. Zanchetta, M. Summer, M. Marinelli and F. Cupertino, "Experimental Modeling and Control Design of Shunt Active Power Filters," *ELSEVIER*

Control Engineering Practice, Vol. 17, No. 10, pp. 1126-1135, Oct. 2009.



Yutthachai Sillapawicharn received the B.Eng degree in electrical engineering from Rajamangala Institute of Technology, Bangkok, Thailand in 1994 and the M.Eng. degree in Electrical Engineering from Chulalongkorn University, Bangkok, Thailand in 1999.

He is currently working toward his Ph.D. at Chiang Mai University. His research interests are in power electronics, and power quality.



Yuttana Kumsuwan received the M.Eng. degree in electrical engineering from King Mongkut's Institute of Technology Ladkrabang, Bangkok, Thailand, in 2000 and the Ph.D. degrees in electrical engineering from Chiang Mai University, Chiang Mai, Thailand, in 2007. Since 2011, he has

been an Assistant Professor in the Department of Electrical Engineering, Chiang Mai University. He was a visiting professor at the Texas A&M University, College Station, United States, from October 2007 to May 2008, and at Ryerson University, Toronto, ON, Canada in March to May 2010. His research interests include power electronics, energy conversion systems, and electric drives.